Dilute neutron star matter from neural-network quantum states

Bryce Fore,[1] Jane M. Kim,[2] Giuseppe Carleo,[3] Morten Hjorth-Jensen,[2,4] Alessandro Lovato,[1,5,6] and Maria Piarulli[7,8]

[1]*Physics Division, Argonne National Laboratory, Argonne, Illinois 60439, USA*
[2]*Department of Physics and Astronomy and Facility for Rare Isotope Beams, Michigan State University, East Lansing, Michigan 48824, USA*
[3]*Institute of Physics, École Polytechnique Fédérale de Lausanne (EPFL), CH-1015 Lausanne, Switzerland*
[4]*Department of Physics and Center for Computing in Science Education, University of Oslo, N-0316 Oslo, Norway*
[5]*Computational Science Division, Argonne National Laboratory, Argonne, Illinois 60439, USA*
[6]*INFN-TIFPA Trento Institute for Fundamental Physics and Applications, 38123 Trento, Italy*
[7]*Physics Department, Washington University, St Louis, Missouri 63130, USA*
[8]*McDonnell Center for the Space Sciences at Washington University in St. Louis, Missouri 63130, USA*

(Received 14 December 2022; accepted 9 July 2023; published 31 July 2023)

Low-density neutron matter is characterized by fascinating emergent quantum phenomena, such as the formation of Cooper pairs and the onset of superfluidity. We model this density regime by capitalizing on the expressivity of the hidden-nucleon neural-network quantum states combined with variational Monte Carlo and stochastic reconfiguration techniques. Our approach is competitive with the auxiliary-field diffusion Monte Carlo method at a fraction of the computational cost. Using a leading-order pionless effective field theory Hamiltonian, we compute the energy per particle of infinite neutron matter and compare it with those obtained from highly realistic interactions. In addition, a comparison between the spin-singlet and triplet two-body distribution functions indicates the emergence of pairing in the $^1S_0$ channel.

DOI: 10.1103/PhysRevResearch.5.033062

I. INTRODUCTION

Multimessenger astronomy has opened new windows into the state of matter at densities and isospin asymmetries that cannot be directly probed by terrestrial experiments [1–4]. Concurrently, nuclear many-body theory has made considerable progress in computing the nucleonic-matter equation of state at densities corresponding to the inner core of neutron stars starting from realistic Hamiltonians [5–10]. Comparisons between theoretical predictions and astrophysical observation pose stringent constraints on models of nuclear dynamics, particularly three-nucleon forces [11].

In this work, we focus on lower densities, $\rho \lesssim 0.08$ fm^{-3}, which are relevant to the phenomenology of the stellar inner crust at the boundary with the outer core. In this region, matter consists of a Coulomb lattice of neutron-rich nuclei, relativistic electrons, and a superfluid neutron gas [12]. In this region, both conditions for superfluidity—strong Fermi degeneracy and an attractive interaction between neutron pairs in the $^1S_0$ channel—are believed to be met [13–15]. In addition to lowering the system's energy, the formation of Cooper pairs plays a critical role in neutrino emission [16,17] and the phenomenology of glitches [18]. Pairing is also relevant in modeling neutron-rich nuclei, which are the subject of intense experimental activities [19].

Quantum Monte Carlo approaches [20], and in particular the auxiliary-field diffusion Monte Carlo (AFDMC) method [21], have been extensively applied to accurately compute neutron-matter properties [6,7,22]. In the low-density regime, AFDMC calculations have convincingly shown a depletion of the superfluid gap with respect to the Bardeen-Cooper-Schrieffer theory [23,24]. However, because of the fermion sign problem, AFDMC predictions depend upon the starting variational wave function. For instance, the superfluid phase must be assumed *a priori* by using Pfaffian wave functions [25].

Neural-network quantum states [26] (NQS) have gained popularity in solving the Schrödinger equation of atomic nuclei both in real space [27–31] and in the occupation-number formalism [32]. In this work, we introduce a periodic NQS suitable to model both the normal and superfluid phases of neutron matter. The ansatz is based on the "hidden-nucleon" architecture, which can model the ground-state wave functions of nuclei up to ^{16}O with high accuracy [30]. Inspired by chemistry applications [33,34], we further improve the expressivity of the hidden-nucleon NQS using generalized backflow correlations, which generalize both the Pfaffian and the spin-dependent backflow of Ref. [35].

Our model of nuclear dynamics is the leading-order pionless effective field theory ($\not\pi$EFT) Hamiltonian of Ref. [36], which qualitatively reproduces the binding energies of nuclei with up to $A = 90$ nucleons. Arguments based on the

expansion around the unitary limit [37], and Brueckner-Hartree-Fock calculations of infinite nuclear matter [38], indicate that $\not\pi$EFT should provide accurate energies of dilute neutron matter. We quantitatively address this point by carrying out variational Monte Carlo calculations based on NQS that are specifically designed to model wave functions of nuclear systems in the presence of spatial periodicity. We compare the $\not\pi$EFT energy per particle against the phenomenological Argonne v_{18} [39] plus Urbana IX [40] (AV18+UIX) Hamiltonian used in the Akmal-Pandharipande-Ravenhall (APR) [41] equation of state. We additionally consider the local, Δ-full chiral-EFT potentials that include tritium β decay in the fitting procedure and do not yield self-bound neutron matter [6,22].

To better quantify the role of dynamical correlations, we evaluate the two-body spatial distribution functions, separating the spin-triplet and spin-singlet channels. We analyze the self-emergence of pairing correlations, not explicitly included in the NQS ansatz, as a function of neutron-matter density.

II. METHODS

We model the interactions among neutrons through the leading-order $\not\pi$EFT Hamiltonian "o" of Ref. [36]. The two-body contact potential is designed to reproduce the np scattering lengths and effective ranges in the $S/T = 0/1$ and $1/0$ channels. Thus it yields a neutron-neutron scattering length of $a_{nn} = -22.5$ fm, slightly larger than the experimental value of $-18.9(4)$ fm, see [42] and references therein, while the effective range is well reproduced. The Hamiltonian also contains a repulsive three-body force that ensures the stability of nuclei with $A \leqslant 3$ nucleons. As for the latter, we take the parametrization with $R_3 = 1.0$ fm, as it reproduces the binding energies of nuclei in the $A \leqslant 90$ mass range reasonably well. For benchmarking purposes, we also consider the leading-order $\not\pi$EFT Hamiltonian "a" with $R_3 = 1.0$ fm, which describes the trend of binding energies of light and medium-mass nuclei.

We approximate the ground-state solution of the nuclear many-body problem with an NQS ansatz that belongs to the hidden-fermion family [43], recently generalized to continuum Hilbert spaces and applied to atomic nuclei in Ref. [30]. In addition to the visible spatial and spin coordinates of the A neutrons, $R = \{\mathbf{r}_1 \dots \mathbf{r}_A\}$ and $S = \{s_1^z \dots s_A^z\}$, the Hilbert space contains fictitious A_h hidden-nucleon degrees of freedom. In this work we use $A_h = A = 14$ so that the system is as flexible as possible, but in practice we have also found using as few as eight hidden nucleons gives very similar results. The wave function can be conveniently expressed in a block matrix form as

$$\Psi_{HN}(R,S) \equiv \det\begin{bmatrix} \phi_v(R,S) & \phi_v(R_h,S_h) \\ \chi_h(R,S) & \chi_h(R_h,S_h) \end{bmatrix}. \tag{1}$$

As in Ref. [30], $\phi_v(R,S)$ is the $A \times A$ matrix representing visible single-particle orbitals computed on the visible coordinates, while the $A_h \times A_h$ matrix $\chi_h(R_h,S_h)$ yields the amplitudes of hidden orbitals evaluated on the coordinates of the A_h hidden nucleons. Finally, $\chi_h(R,S)$ and $\phi_v(R_h,S_h)$ are $A_h \times A$ and $A \times A_h$ matrices giving the amplitudes of hidden orbitals on visible coordinates and visible orbitals on hidden coordinates, respectively. All the above matrices are expressed in terms of deep neural networks with differentiable activation functions—see Ref. [30] for additional details. To respect the Pauli principle, the coordinates of the hidden nucleons must be permutation-invariant functions of the visible ones. We enforce this symmetry by using a Deep-Sets architecture [44,45] with *logsumexp* pooling. Additionally, the discrete parity and time reversal symmetries are enforced in the same manner as Ref. [30].

Inspired by recent developments in quantum-chemistry NQS [33,34,46], we augment the flexibility of the ansatz by performing a generalized backflow transformation to the visible coordinates of the hidden-nucleon matrix: $(R,S) \to (\tilde{R},\tilde{S})$. The backflow transformations generate new coordinates that are equivariant with respect to the original one, ensuring that the NQS ansatz maintains fermion antisymmetry. This is accomplished by using the Deep-Sets architecture to define

$$\Phi_i = \ln\left(\sum_j \exp\left[\phi_{\mathrm{bf,i}}(\mathbf{r}_j, s_j^z)\right]\right). \tag{2}$$

Because of the sum over all particles, Φ_i is independent of their ordering. The latter is restored by concatenating it with the corresponding particle coordinates

$$\left(\tilde{\mathbf{r}}_i, \tilde{s}_i^z\right) = \rho_{\mathrm{bf,i}}\left(\mathbf{r}_i, s_i^z, \Phi_i\right). \tag{3}$$

To enhance the expressivity of the ansatz, separate ρ_{bf} and ϕ_{bf} neural networks are used for each of the A visible orbitals.

We simulate infinite neutron matter using 14 particles in a box with periodic boundary conditions. Following Ref. [47], the latter are imposed by mapping the spatial coordinates onto periodic functions by

$$\boldsymbol{r}_i \to \left[\sin\left(\frac{2\pi \boldsymbol{r}_i}{L}\right), \cos\left(\frac{2\pi \boldsymbol{r}_i}{L}\right)\right], \tag{4}$$

which ensures the wave function is continuous and differentiable at the box boundary. Here L is the size of the simulation periodic box and the sin and cos functions are applied elementwise to $\boldsymbol{r}_i$. Finite-size effects due to the tail corrections of two- and three-body potentials are accounted for by summing the contributions given by neighboring cells to the simulation box [48].

Evaluating the expectation values of quantum-mechanical operators, including the Hamiltonian, requires carrying out multidimensional integration over the spatial and spin coordinates of the neutrons. To this aim, we exploit Monte Carlo quadrature and sample R and S from $|\Psi_{HN}(R,S)|^2$ using the Metropolis-Hastings algorithm [49]—additional details can be found in the Supplemental Material of Ref. [28]. The best variational parameters defining the NQS are found by minimizing the system's energy, which we carry out using the R(oot)M(ean)S(quared)Prop(agation)-enhanced version of the stochastic-reconfiguration optimization method introduced in Ref. [30]. The parameters are updated as

$$\boldsymbol{p} \leftarrow \boldsymbol{p} - \eta S^{-1} \nabla_{\boldsymbol{p}} E, \tag{5}$$

where $E = \langle \Psi_{HN}|H|\Psi_{HN}\rangle / \langle \Psi_{HN}|\Psi_{HN}\rangle$ is the Hamiltonian expectation value, η is the learning rate, and S is the quantum geometric tensor [50].

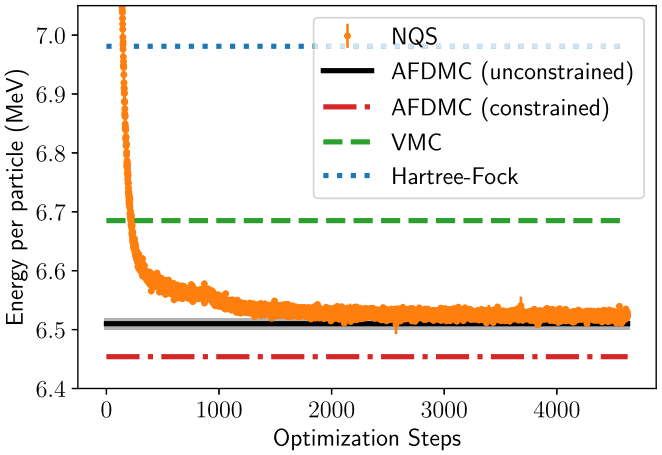

FIG. 1. NQS training data in neutron matter at $\rho = 0.04$ fm^{-3} (data points) compared with Hartree-Fock (dotted line), conventional VMC (dashed line), constrained-path ADMC (dash-dotted line), and unconstrained-path ADMC results (solid line).

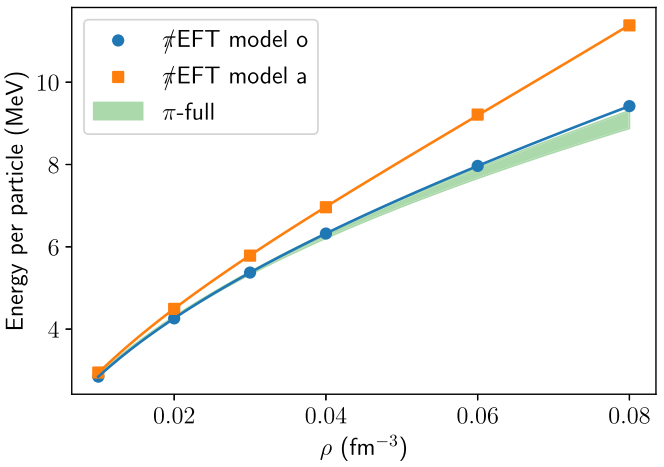

FIG. 2. Low-density neutron-matter $\not\pi$EFT equation of state as obtained with the hidden-nucleon NQS for $\not\pi$EFT potential "o" (blue circles) and $\not\pi$EFT potential "a" (orange squares) compared with interactions which retain pion-exchange terms (green band).

III. RESULTS

We first benchmark the expressivity of the hidden-nucleon NQS for periodic systems by comparing the energy per particle of infinite neutron matter against "conventional" variational Monte Carlo (VMC) and both constrained-path and AFDMC results. The variational wave function used in state-of-the-art neutron-matter studies, see for example [7,22], contains a spin-independent Jastrow factor that multiplies a Slater determinant augmented by spin-dependent backflow correlations. The constrained-path approximation, commonly employed to alleviate the AFDMC fermion-sign problem [20], brings about a bias in the ground-state energy estimate [6,22]. Exact results can be obtained by performing unconstrained propagations, but the statistical error grows exponentially with the imaginary time.

As shown in Fig. 1 for $\rho = 0.04$ fm^{-3}, after $\simeq$2000 stochastic-reconfiguration steps, the NQS ansatz converges to the *virtually exact* unconstrained AFDMC energy, using a fraction of its computing time: about 100 h on NVIDIA-A100 GPUs vs approximately 1.2 million h on Intel-KNL CPUs. Notice that the constrained-path approximation violates the variational principle. In contrast, variational Monte Carlo calculations based on the NQS never yield energies below that of the Hamiltonian's ground state. Comparing with the Hartree-Fock approximation, it appears that the hidden-nucleon ansatz captures the overwhelming majority of the correlation energy.

In Fig. 2, we compare the $\not\pi$EFT energies obtained with the NQS ansatz against AFDMC calculations of 14 particles with periodic-box boundary conditions, so that finite-size effects are the same in both approaches. To mitigate these effects, in addition to the tail corrections of two- and three-body potentials, we subtract the kinetic energy of 14 particles in a box and add the kinetic energy computed in the thermodynamic limit [51]. We assess the accuracy of this procedure by comparing the Hartree-Fock energy in the thermodynamic limit with calculations performed using 14 particles in a periodic box and plane-wave orbitals, with the kinetic energy contribution corrected as described above. The "corrected" energy closely aligns with the thermodynamic limit for all densities considered, with a maximum deviation remaining below 1%.

The AFDMC takes as input the AV18+UIX Hamiltonian used in the celebrated APR equation of state [41] and the local, Δ-full chiral-EFT potentials that include tritium β decay in the fitting procedure and do not make neutron-matter collapse, i.e., models NV2+3-Ia*/b*, and NV2+3-IIb* [6,22]. Since for all the densities we consider, the AV18+UIX, NV2+3-Ia*/b*, and NV2+3-IIb* are in excellent agreement, they are collectively displayed by the "π-full" band, stressing that all these interactions explicitly retain pion-exchange terms.

The $\not\pi$EFT Hamiltonian "o" is in excellent agreement with the π-full models—both providing energies much below the noninteracting Fermi gas (not shown in the figure). These minor differences are likely because model "o" yields a slightly larger *nn* scattering length than the experimental value and, therefore, more attraction in neutron matter. For benchmark purposes, we also consider the $\not\pi$EFT model "a" of Ref. [36], which provides a slightly stiffer equation of state than model "o." By checking the individual expectation value of the two- and three-body potentials, we find that this behavior is primarily due to the three-body force contribution that is more repulsive in model "a" than model "o," which arises from a more bound ^{3}H when the two-body force alone is employed.

Once trained on the system's energy, the NQS can be used to accurately evaluate a variety of quantum-mechanical observables, such as the spin-singlet and -triplet two-body distribution functions defined in Ref. [52]. Figure 3 shows these distributions at $\rho = 0.01$ fm^{-3} [panel (a)], $\rho = 0.04$ fm^{-3} [panel (b)], and $\rho = 0.08$ fm^{-3} [panel (c)]. The significant increase in the spin-singlet channel compared to the noninteracting Fermi gas indicates that the NQS wave function can capture the emergence of the $^1S_0$ neutron pairing, despite not being explicitly encoded in the ansatz. Consistent with the behavior of the pairing gap [14,23], the enhancement is more prominent at low densities and vanishes at higher densities.

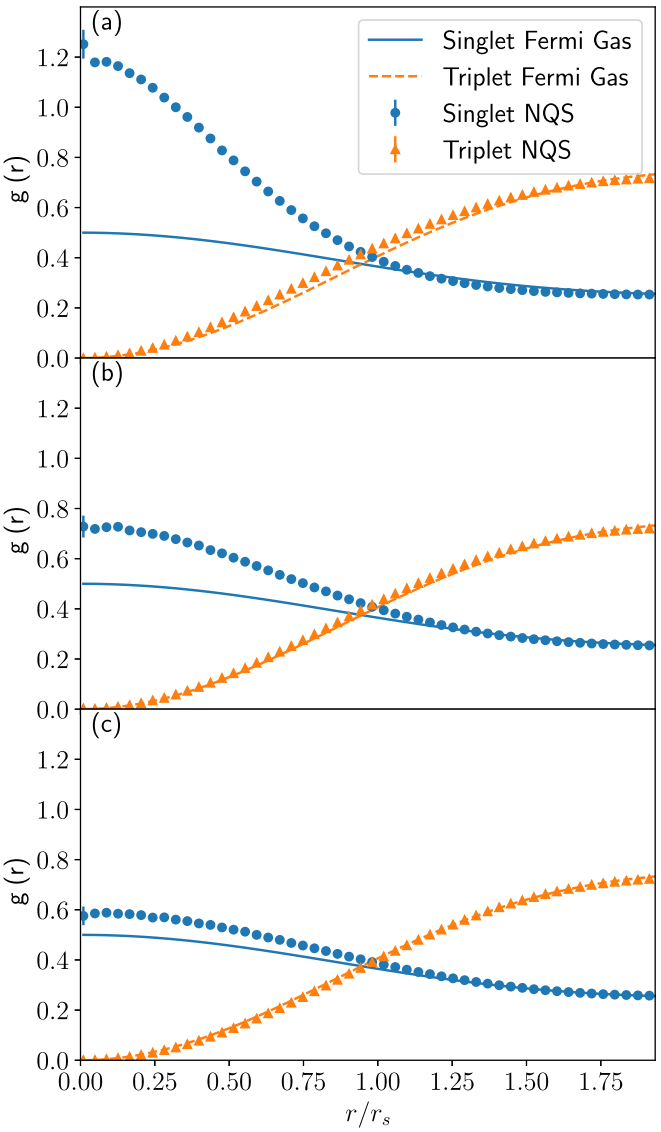

FIG. 3. Spin-singlet and triplet two-body distribution functions at $\rho = 0.01$ fm^{-3} [panel (a)], $\rho = 0.04$ fm^{-3} [panel (b)], and $\rho = 0.08$ fm^{-3} [panel (c)] vs pair distance in units of the Wigner-Seitz radius. The NQS calculations (solid symbols) are compared with noninteracting Fermi gas results (solid lines).

On the other hand, at these densities, no pairing correlations are present in the spin-triplet channel.

IV. CONCLUSIONS

In this work, we have put forward an NQS suitable to model the normal and superfluid phases of infinite neutron matter in a unified fashion. We improve the expressivity of the hidden-nucleon ansatz of Ref. [30] by adding state-dependent generalized backflow correlations, whose inclusion has proven beneficial in condensed-matter applications [33,34]. Periodic-box boundary conditions are imposed by mapping the spatial coordinates of the neutrons onto periodic functions.

Combined with Monte Carlo techniques to sample the Hilbert space and the stochastic-reconfiguration algorithm to optimize the variational parameters, the NQS yields energies per particle of low-density neutron matter that are in excellent agreement with unconstrained AFDMC calculations at a fraction of the computational cost. In contrast, the computationally inexpensive AFDMC constrained-path approximation brings about appreciable violations of the variational principle.

We have shown that $\not\pi$EFT yields a low-density neutron matter equation of state that is remarkably close to those obtained from AFDMC calculations that take as input highly realistic phenomenological and chiral-EFT interactions [6,22,41]. This finding paves the way for more systematic comparisons between dilute neutron matter and Fermi gas around the unitary limit. In addition, it enables studies of phenomena relevant to understanding the inner crust and the outer core of neutron stars, such as pairing and superfluidity, using relatively simple models of nuclear dynamics.

Finally, we have analyzed the possible onset of Cooper pairing in the neutron medium. Specifically, the NQS two-body distribution functions corresponding to pairs of neutrons in the spin-singlet $^1S_0$ channel exhibit a clear enhancement at small interparticle distances with respect to the noninteracting case, which is absent in the spin-triplet channel. Consistent with pairing-gap calculations [14,23,24], this behavior is more prominent at smaller densities. Note that this feature has not been encoded in the NQS; rather, it is a self-emerging quantum-mechanical phenomenon.

As a future development, we plan on including more sophisticated interactions, including highly realistic phenomenological ones, including AV18+UIX and the local, Δ-full chiral-EFT potentials of Refs. [6,22,53]. The flexibility of the NQS ansatz will also be tested in isospin-asymmetric nucleonic matter at low densities, where strong clustering is expected to occur [54].

ACKNOWLEDGMENTS

We are grateful to O. Benhar, S. Gandolfi, A. Kievsky, and B. Wiringa for many illuminating discussions. A.L. and B.F. are supported by the US Department of Energy, Office of Science, Office of Nuclear Physics, under Contract No. DE-AC02-06CH11357, by the 2020 DOE Early Career Award No. ANL PRJ1008597, by the NUCLEI SciDAC program, and Argonne LDRD awards. M.P. is supported by the 2021 Early Career Award No. DE-SC0022002 and the FRIB Theory Alliance Award No. DE-SC0013617. J.M.K. and M.H.-J. are supported by the US National Science Foundation Grants No. PHY-1404159 and No. PHY-2013047. Numerical calculations were performed using resources of the Laboratory Computing Resource Center at Argonne National Laboratory and the computers of the Argonne Leadership Computing Facility via the ALCC grant "Short Range Correlations from a Quantum Monte Carlo perspective."

[1] B. P. Abbott *et al.* (LIGO Scientific Collaboration and Virgo Collaboration), GW170817: Observation of Gravitational Waves from a Binary Neutron Star Inspiral, Phys. Rev. Lett. **119**, 161101 (2017).

[2] B. P. Abbott *et al.* (LIGO Scientific Collaboration and Virgo Collaboration), Multi-messenger observations of a binary neutron star merger, Astrophys. J. **848**, L12 (2017).

[3] A. Sabatucci and O. Benhar, Tidal deformation of neutron stars from microscopic models of nuclear dynamics, Phys. Rev. C **101**, 045807 (2020).

[4] P. Senger, Probing dense nuclear matter in the laboratory: Experiments at fair and nica, Universe **7**, 171 (2021).

[5] C. Drischler, A. Carbone, K. Hebeler, and A. Schwenk, Neutron matter from chiral two- and three-nucleon calculations up to N^3LO, Phys. Rev. C **94**, 054307 (2016).

[6] M. Piarulli, I. Bombaci, D. Logoteta, A. Lovato, and R. B. Wiringa, Benchmark calculations of pure neutron matter with realistic nucleon-nucleon interactions, Phys. Rev. C **101**, 045801 (2020).

[7] D. Lonardoni, I. Tews, S. Gandolfi, and J. Carlson, Nuclear and neutron-star matter from local chiral interactions, Phys. Rev. Res. **2**, 022033(R) (2020).

[8] W. G. Jiang, A. Ekström, C. Forssén, G. Hagen, G. R. Jansen, and T. Papenbrock, Accurate bulk properties of nuclei from $A = 2$ to ∞ from potentials with Δ isobars, Phys. Rev. C **102**, 054301 (2020).

[9] F. Sammarruca and R. Millerson, Overview of symmetric nuclear matter properties from chiral interactions up to fourth order of the chiral expansion, Phys. Rev. C **104**, 064312 (2021).

[10] H. Heiselberg and M. Hjorth-Jensen, Phases of dense matter in neutron stars, Phys. Rep. **328**, 237 (2000).

[11] A. Sabatucci, O. Benhar, A. Maselli, and C. Pacilio, Sensitivity of neutron star observations to three-nucleon forces, Phys. Rev. D **106**, 083010 (2022).

[12] I. Vidaña, Low-density neutron matter and the unitary limit, Front. Phys. **9**, 170 (2021).

[13] A. Sedrakian, J. W. Clark, and M. Alford, *Pairing in Fermionic Systems* (World Scientific, Singapore, 2006).

[14] O. Benhar and G. De Rosi, Superfluid gap in neutron matter from a microscopic effective interaction, J. Low Temp. Phys. **189**, 250 (2017).

[15] D. J. Dean and M. Hjorth-Jensen, Pairing in nuclear systems: from neutron stars to finite nuclei, Rev. Mod. Phys. **75**, 607 (2003).

[16] D. G. Yakovlev and C. J. Pethick, Neutron star cooling, Annu. Rev. Astron. Astrophys. **42**, 169 (2004).

[17] D. Page, M. Prakash, J. M. Lattimer, and A. W. Steiner, Rapid Cooling of the Neutron Star in Cassiopeia A Triggered by Neutron Superfluidity in Dense Matter, Phys. Rev. Lett. **106**, 081101 (2011).

[18] C. Monrozeau, J. Margueron, and N. Sandulescu, Nuclear superfluidity and cooling time of neutron-star crust, Phys. Rev. C **75**, 065807 (2007).

[19] F. Nowacki, A. Obertelli, and A. Poves, The neutron-rich edge of the nuclear landscape: Experiment and theory, Prog. Part. Nucl. Phys. **120**, 103866 (2021).

[20] J. Carlson, S. Gandolfi, F. Pederiva, S. C. Pieper, R. Schiavilla, K. E. Schmidt, and R. B. Wiringa, Quantum Monte Carlo methods for nuclear physics, Rev. Mod. Phys. **87**, 1067 (2015).

[21] K. E. Schmidt and S. Fantoni, A quantum Monte Carlo method for nucleon systems, Phys. Lett. B **446**, 99 (1999).

[22] A. Lovato, I. Bombaci, D. Logoteta, M. Piarulli, and R. B. Wiringa, Benchmark calculations of infinite neutron matter with realistic two- and three-nucleon potentials, Phys. Rev. C **105**, 055808 (2022).

[23] S. Gandolfi, A. Yu. Illarionov, S. Fantoni, F. Pederiva, and K. E. Schmidt, Equation of State of Superfluid Neutron Matter and the Calculation of $^1S_0$ Pairing Gap, Phys. Rev. Lett. **101**, 132501 (2008).

[24] S. Gandolfi, G. Palkanoglou, J. Carlson, A. Gezerlis, and K. E. Schmidt, The $^1S_0$ pairing gap in neutron matter, Condens. Matter **7**, 19 (2022).

[25] M. Bajdich, L. Mitas, G. Drobny, L. K. Wagner, and K. E. Schmidt, Pfaffian Pairing Wave Functions in Electronic-Structure Quantum Monte Carlo Simulations, Phys. Rev. Lett. **96**, 130201 (2006).

[26] G. Carleo and M. Troyer, Solving the quantum many-body problem with artificial neural networks, Science **355**, 602 (2017).

[27] J. W. T. Keeble and A. Rios, Machine learning the deuteron, Phys. Lett. B **809**, 135743 (2020).

[28] C. Adams, G. Carleo, A. Lovato, and N. Rocco, Variational Monte Carlo Calculations of $A \leqslant 4$ Nuclei with an Artificial Neural-Network Correlator Ansatz, Phys. Rev. Lett. **127**, 022502 (2021).

[29] A. Gnech, C. Adams, N. Brawand, G. Carleo, A. Lovato, and N. Rocco, Nuclei with up to $A = 6$ nucleons with artificial neural network wave functions, Few Body Syst. **63**, 7 (2022).

[30] A. Lovato, C. Adams, G. Carleo, and N. Rocco, Hidden-nucleons neural-network quantum states for the nuclear many-body problem, Phys. Rev. Res. **4**, 043178 (2022).

[31] Y. L. Yang and P. W. Zhao, A consistent description of the relativistic effects and three-body interactions in atomic nuclei, Phys. Lett. B **835**, 137587 (2022).

[32] M. Rigo, B. Hall, M. Hjorth-Jensen, A. Lovato, and F. Pederiva, Solving the nuclear pairing model with neural network quantum states, Phys. Rev. E **107**, 025310 (2023).

[33] J. Hermann, Z. Schätzle, and F. Noé, Deep-neural-network solution of the electronic Schrödinger equation, Nat. Chem. **12**, 891 (2020).

[34] D. Pfau, J. S. Spencer, A. G. D. G. Matthews, and W. M. C. Foulkes, *Ab initio* solution of the many-electron Schrödinger equation with deep neural networks, Phys. Rev. Res. **2**, 033429 (2020).

[35] L. Brualla, S. Fantoni, A. Sarsa, K. E. Schmidt, and S. A. Vitiello, Spin orbit induced backflow in neutron matter with auxiliary field diffusion Monte Carlo, Phys. Rev. C **67**, 065806 (2003).

[36] R. Schiavilla, L. Girlanda, A. Gnech, A. Kievsky, A. Lovato, L. E. Marcucci, M. Piarulli, and M. Viviani, Two- and three-nucleon contact interactions and ground-state energies of light- and medium-mass nuclei, Phys. Rev. C **103**, 054003 (2021).

[37] S. König, H. W. Grießhammer, H. W. Hammer, and U. van Kolck, Nuclear Physics Around the Unitarity Limit, Phys. Rev. Lett. **118**, 202501 (2017).

[38] A. Kievsky, M. Viviani, D. Logoteta, I. Bombaci, and L. Girlanda, Correlations Imposed by the Unitary Limit between Few-Nucleon Systems, Nuclear Matter and Neutron Stars, Phys. Rev. Lett. **121**, 072701 (2018).

[39] R. B. Wiringa, V. G. J. Stoks, and R. Schiavilla, Accurate nucleon-nucleon potential with charge independence breaking, Phys. Rev. C **51**, 38 (1995).

[40] B. S. Pudliner, V. R. Pandharipande, J. Carlson, and R. B. Wiringa, Quantum Monte Carlo Calculations of $A \leqslant 6$ Nuclei, Phys. Rev. Lett. **74**, 4396 (1995).

[41] A. Akmal, V. R. Pandharipande, and D. G. Ravenhall, Equation of state of nucleon matter and neutron star structure, Phys. Rev. C **58**, 1804 (1998).

[42] R. Machleidt and D. R. Entem, Chiral effective field theory and nuclear forces, Phys. Rep. **503**, 1 (2011).

[43] J. R. Moreno, G. Carleo, A. Georges, and J. Stokes, Fermionic wave functions from neural-network constrained hidden states, Proc. Natl. Acad. Sci. USA **119**, e2122059119 (2022).

[44] M. Zaheer, S. Kottur, S. Ravanbakhsh, B. Poczos, R. Salakhutdinov, and A. Smola, Deep sets, arXiv:1703.06114.

[45] E. Wagstaff, F. B. Fuchs, M. Engelcke, I. Posner, and M. Osborne, On the limitations of representing functions on sets, arXiv:1901.09006, http://proceedings.mlr.press/v97/wagstaff19a/wagstaff19a.pdf.

[46] Di. Luo and B. K. Clark, Backflow Transformations via Neural Networks for Quantum Many-Body Wave Functions, Phys. Rev. Lett. **122**, 226401 (2019).

[47] G. Pescia, J. Han, A. Lovato, J. Lu, and G. Carleo, Neural-network quantum states for periodic systems in continuous space, Phys. Rev. Res. **4**, 023138 (2022).

[48] A. Sarsa, S. Fantoni, K. E. Schmidt, and F. Pederiva, Neutron matter at zero temperature with auxiliary field diffusion Monte Carlo, Phys. Rev. C **68**, 024308 (2003).

[49] N. Metropolis, A. W. Rosenbluth, M. N. Rosenbluth, A. H. Teller, and E. Teller, Equation of state calculations by fast computing machines, J. Chem. Phys. **21**, 1087 (1953).

[50] J. Stokes, J. Izaac, N. Killoran, and G. Carleo, Quantum natural gradient, Quantum **4**, 269 (2020).

[51] S. Gandolfi, A. Lovato, J. Carlson, and K. E. Schmidt, From the lightest nuclei to the equation of state of asymmetric nuclear matter with realistic nuclear interactions, Phys. Rev. C **90**, 061306(R) (2014).

[52] S. Gandolfi, A. Y. Illarionov, F. Pederiva, K. E. Schmidt, and S. Fantoni, Equation of state of low-density neutron matter, and the $^1S_0$ pairing gap, Phys. Rev. C **80**, 045802 (2009).

[53] M. Piarulli *et al.*, Light-Nuclei Spectra from Chiral Dynamics, Phys. Rev. Lett. **120**, 052503 (2018).

[54] J. W. Negele and D. Vautherin, Neutron star matter at subnuclear densities, Nucl. Phys. A **207**, 298 (1973).